



**HAL**  
open science

## **HD 50844: a new look at delta Scuti stars from CoRoT space photometry**

Ennio Poretti, Eric Michel, Rafael Garrido, Laure Lefèvre, L. Mantegazza,  
Monica Rainer, E. Rodríguez, K. Uytterhoeven, Pedro J. Amado, Susana  
Martin-Ruiz, et al.

► **To cite this version:**

Ennio Poretti, Eric Michel, Rafael Garrido, Laure Lefèvre, L. Mantegazza, et al.. HD 50844: a new look at delta Scuti stars from CoRoT space photometry. *Astronomy and Astrophysics - A&A*, 2009, 506, pp.85-93. 10.1051/0004-6361/200912039 . hal-03785129

**HAL Id: hal-03785129**

**<https://hal.science/hal-03785129>**

Submitted on 8 Oct 2022

**HAL** is a multi-disciplinary open access archive for the deposit and dissemination of scientific research documents, whether they are published or not. The documents may come from teaching and research institutions in France or abroad, or from public or private research centers.

L'archive ouverte pluridisciplinaire **HAL**, est destinée au dépôt et à la diffusion de documents scientifiques de niveau recherche, publiés ou non, émanant des établissements d'enseignement et de recherche français ou étrangers, des laboratoires publics ou privés.

## HD 50844: a new look at $\delta$ Scti stars from CoRoT space photometry<sup>★, ★★</sup>

E. Poretti<sup>1</sup>, E. Michel<sup>2</sup>, R. Garrido<sup>3</sup>, L. Lefèvre<sup>2</sup>, L. Mantegazza<sup>1</sup>, M. Rainer<sup>1</sup>, E. Rodríguez<sup>3</sup>, K. Uytterhoeven<sup>1,★★★</sup>, P. J. Amado<sup>3</sup>, S. Martín-Ruiz<sup>3</sup>, A. Moya<sup>3</sup>, E. Niemczura<sup>4</sup>, J. C. Suárez<sup>3</sup>, W. Zima<sup>5</sup>, A. Baglin<sup>2</sup>, M. Auvergne<sup>2</sup>, F. Baudin<sup>6</sup>, C. Catala<sup>2</sup>, R. Samadi<sup>2</sup>, M. Alvarez<sup>7</sup>, P. Mathias<sup>8</sup>, M. Paparò<sup>9</sup>, P. Pápics<sup>9</sup>, and E. Plachy<sup>9</sup>

<sup>1</sup> INAF – Osservatorio Astronomico di Brera, via E. Bianchi 46, 23807 Merate (LC), Italy  
e-mail: ennio.poretti@brera.inaf.it

<sup>2</sup> LESIA, Observatoire de Paris, CNRS (UMR 8109), Université Paris 6, Université Paris Diderot, 5 place J. Janssen, 92195 Meudon, France

<sup>3</sup> Instituto de Astrofísica de Andalucía, Apartado 3004, 18080 Granada, Spain

<sup>4</sup> Astronomical Institute of the Wrocław University, ul. Kopernika 11, 51-622 Wrocław, Poland

<sup>5</sup> Instituut voor Sterrenkunde, K.U. Leuven, Celestijnenlaan 200 D, 3001 Leuven, Belgium

<sup>6</sup> Institut d'Astrophysique Spatiale, CNRS, UMR 8617, Université Paris XI, 91405 Orsay, France

<sup>7</sup> Observatorio Astronómico Nacional, Instituto de Astronomía, UNAM, Apto Postal 877, Ensenada, BC 22860, Mexico

<sup>8</sup> UMR 6525 H. Fizeau, UNS, CNRS, OCA, Campus Valrose, 06108 Nice Cedex 2, France

<sup>9</sup> Konkoly Observatory, PO Box 67, 1525 Budapest, Hungary

Received 11 March 2009 / Accepted 10 May 2009

### ABSTRACT

**Aims.** This work presents the results obtained by CoRoT on HD 50844, the only  $\delta$  Sct star observed in the CoRoT initial run (57.6 d). The aim of these CoRoT observations was to investigate and characterize for the first time the pulsational behaviour of a  $\delta$  Sct star, when observed at a level of precision and with a much better duty cycle than from the ground.

**Methods.** The 140 016 datapoints were analysed using independent approaches (SigSpec software and different iterative sine-wave fittings) and several checks performed (splitting of the timeseries in different subsets, investigation of the residual light curves and spectra). A level of  $10^{-5}$  mag was reached in the amplitude spectra of the CoRoT timeseries. The space monitoring was complemented by ground-based high-resolution spectroscopy, which allowed the mode identification of 30 terms.

**Results.** The frequency analysis of the CoRoT timeseries revealed hundreds of terms in the frequency range 0–30 d<sup>-1</sup>. All the cross-checks confirmed this new result. The initial guess that  $\delta$  Sct stars have a very rich frequency content is confirmed. The spectroscopic mode identification gives theoretical support since very high-degree modes (up to  $\ell = 14$ ) are identified. We also prove that cancellation effects are not sufficient in removing the flux variations associated to these modes at the noise level of the CoRoT measurements. The ground-based observations indicate that HD 50844 is an evolved star that is slightly underabundant in heavy elements, located on the Terminal Age Main Sequence. Probably due to this unfavourable evolutionary status, no clear regular distribution is observed in the frequency set. The predominant term ( $f_1 = 6.92$  d<sup>-1</sup>) has been identified as the fundamental radial mode combining ground-based photometric and spectroscopic data.

**Key words.** stars: variables:  $\delta$  Sct – stars: oscillations – stars: interiors – stars: individual: HD 50844

### 1. Introduction

Discovered during the preparatory work of the CoRoT mission, HD 50844 was observed during the initial run (IR01). It is a slightly evolved star, close to the Terminal Age Main Sequence. The physical parameters derived from Strömrgren photometry are  $M_V = 1.31$ ,  $T_{\text{eff}} = 7500$  K,  $\log g = 3.6$ , and  $[\text{Fe}/\text{H}] = -0.4$  dex (Poretti et al. 2005). In this paper we review our understanding of  $\delta$  Sct stars and unveil a new “look” of their frequency spectra, thanks to the intensive CoRoT monitoring. We also try to answer some open questions on mode excitation in the pulsators located in the lower part of the instability strip. To give as complete as possible answers, we also obtained high-resolution spectroscopy and multicolour photometry from ground. In particular, the study of line profile variations is a complementary approach, and essential for the identification of the excited modes.

\* The CoRoT space mission was developed and is operated by the French space agency CNES, with participation of ESA's RSSD and Science Programmes, Austria, Belgium, Brazil, Germany, and Spain. This work is based on ground-based observations made with ESO telescopes at the La Silla Observatory under the ESO Large Programme LP178.D-0361 and on data collected at the Observatorio de Sierra Nevada (Spain), at the Observatorio Astronómico Nacional San Pedro Mártir (Mexico), and at the Pizskéstető Mountain Station of Konkoly Observatory (Hungary).

\*\* Table 2 is only available in electronic form at the CDS via anonymous ftp to cdsarc.u-strasbg.fr (130.79.128.5) or via <http://cdsweb.u-strasbg.fr/cgi-bin/qcat?J/A+A/506/85>

\*\*\* Current address: Laboratoire AIM, CEA/DSM CNRS Université Paris Diderot, CEA, IRFU, SAp, centre de Saclay, 91191 Gif-sur-Yvette, France.

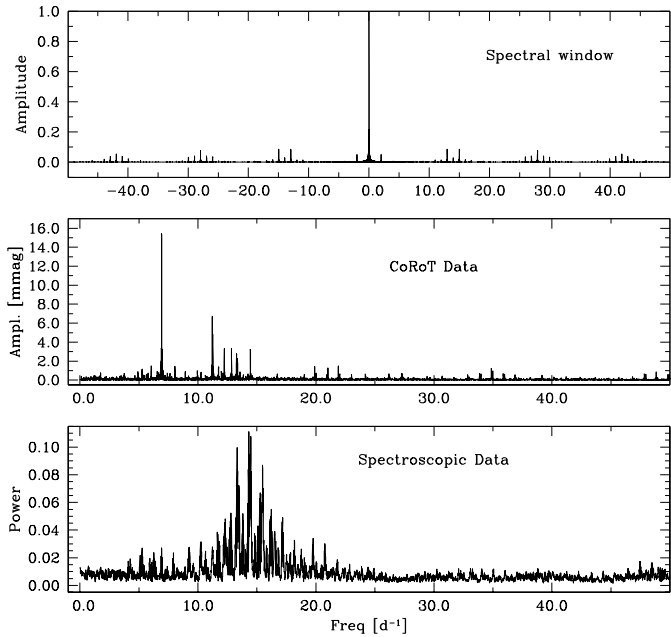


**Fig. 1.** *Top panel:* the spectral window of the CoRoT data on HD 50844, observed in the Initial Run of the mission. *Middle panel:* the amplitude spectrum of the original CoRoT data. *Bottom panel:* the power spectrum (in units of the normalized spectral power) of the line profile variations detected in the ground-based spectroscopic data.

## 2. The CoRoT data

The IR01 started on February 2nd, 2007 and finished on March 31st, 2007 ( $\Delta T = 57.61$  d). The exposure time in the CoRoT asteroseismology channel is 1 s. For the analysis, we used the reduced N2 data rebinned at 32 s and we only considered the 140 016 datapoints for which no problem (i.e., flag = 0) were reported. The amplitudes of the background orbital variations are kept at a very small level by the great effectiveness of the baffle (Auvergne et al. 2009). The subsequent rejection of the uncertain points strongly minimized the orbital effects. The light curve was detrended with a linear fit to remove the effect of ageing (Auvergne et al. 2009). The 32-s time binning provided an oversampling of the light curve coverage. Therefore, to gain in CPU time and to reduce the noise level, we grouped the original data into new bins of four consecutive measurements, thus obtaining 32 433 datapoints.

The spectral window is shown in Fig. 1. The rejection of the flagged points resulted in a slight enhancement of the amplitude of the orbital frequency, since the bad measurements occurred mostly when the satellite crossed the South Atlantic Anomaly (SAA). This crossing occurred twice in a sidereal day and gave rise to an additional alias peak. In the 0–50  $d^{-1}$  interval, there are four structures in the spectral window. The first is composed of a peak at  $2.006 d^{-1}$  (4% of the amplitude) and of a lower one at  $4.007 d^{-1}$  (0.7% of the amplitude). The second and most prominent structure is around the orbital frequency  $f_s = 13.972 d^{-1}$ :  $f_s$  (3.0% of the amplitude),  $f_s + 1 d^{-1}$  (7.5%) and  $f_s - 1 d^{-1}$  (8.5%). Other structures occur around  $2f_s$  (7.0% of the amplitude), flanked by lower peaks at  $2f_s \pm 1 d^{-1}$  and  $2f_s \pm 2 d^{-1}$ , and around  $3f_s$  (5.0% of the amplitude), flanked by lower peaks at  $3f_s \pm 1 d^{-1}$  and  $3f_s \pm 2 d^{-1}$ .

Several approaches were used to process the CoRoT data, e.g., Period04 (Lenz & Breger 2005), iterative sine-wave

fitting (Vaníček 1971) and SigSpec (Reegen 2007). Moreover, we refined the classical fitting proposed by Vaníček (1971) for the analysis of the CoRoT data on classical pulsators with a Levenberg-Marquardt algorithm. It uses the frequency domain as a first guess for the fitting of sinusoids in the time domain (Lefèvre & Chené 2009).

Although small differences in the values of the detected frequencies have been found (see Sect. 3), the main results described here are independent from the approach used. The presence of the predominant term suggested in the preparatory work, based only on ground-based data ( $f_1 = 6.92 d^{-1}$ , see Fig. 5 in Poretti et al. 2005), has been immediately confirmed. The alias structures of this term (e.g.,  $f_1 + f_s = 20.89$ ,  $f_1 + 2f_s = 34.86$ , and  $f_1 + 3f_s = 48.83 d^{-1}$ ) are visible in the amplitude spectrum of the original data (Fig. 1, middle panel). Both methods were very effective in removing the alias structures together with the real peak; actually, no relevant term is found at the alias frequencies of  $f_1$ . Taking the excellent quality of the N2 data into account, there is little influence of the satellite’s orbital period on the detected frequencies; in particular, those specifically discussed in the paper are free of any aliasing or orbital effect.

## 3. The frequency content of the CoRoT data

To have a reference frame for interpreting of the results for HD 50844 (A2,  $V = 9.09$ ), we also considered the data of HD 292790 (F8,  $V = 9.48$ ), which was observed by CoRoT in the same IR01. Our frequency analysis shows that the luminosity of HD 292790 is modulated by the rotation in a simple way. The amplitude spectrum shows the rotational frequency, its harmonics and the satellite frequencies (Fig. 3, top panel). For most part of the spectrum, i.e., from 10 to 100  $d^{-1}$ , the noise level is distributed in an uniform way and is very low, namely below 0.01 mmag. For  $f < 5 d^{-1}$ , where the modulation terms and the long term drift are concentrated, the noise level increases slightly.

In contrast, the amplitude spectrum of HD 50844 appears to be very dense (Fig. 1, middle panel, and, in a more striking way, Fig. 3, second panel). At first glance, it is clear that the amplitude spectrum of HD 50844 is only for  $f > 50 d^{-1}$  as flat as that of HD 292790. We can calculate a noise amplitude of  $7.5 \times 10^{-6}$  mag. It is straightforward to deduce that the signal is concentrated in the  $f < 30 d^{-1}$  domain, though there is no predominant peak region after identification of 250 frequencies (residual rms 1.2 mmag). At that point, the average peak height (0.10 mmag) for  $f < 30 d^{-1}$  is still 10 times higher than for  $f > 50 d^{-1}$ . A huge number of terms is necessary to reduce the amplitude spectrum of HD 50844 at the expected noise level. The peak height gets progressively lower after the identification of 500, 750, and 1000 terms (third, fourth, and fifth panels in Fig. 3, respectively; see also the second column of Table 1), but the residual rms decreases very slowly (third column of Table 1). Again, many low-amplitude peaks are necessary to reduce the residual rms: after detection of 500 frequencies, other 500 frequencies with amplitudes between 0.06 and 0.03 mmag are needed to reduce the residual rms by a factor of 0.60%.

The distribution of the frequencies offers some clues about the nature of the signal. We calculated the distribution of all the frequencies, of the first 300 in order of detection and of those detected after the 300th rank (Fig. 4). The distribution of all the frequencies is almost flat in the 0–20  $d^{-1}$  region, followed by a slow decline until 30  $d^{-1}$ . This tail is absent in the distribution of the first 300 frequencies, and there is a sharp step at 20  $d^{-1}$ . The

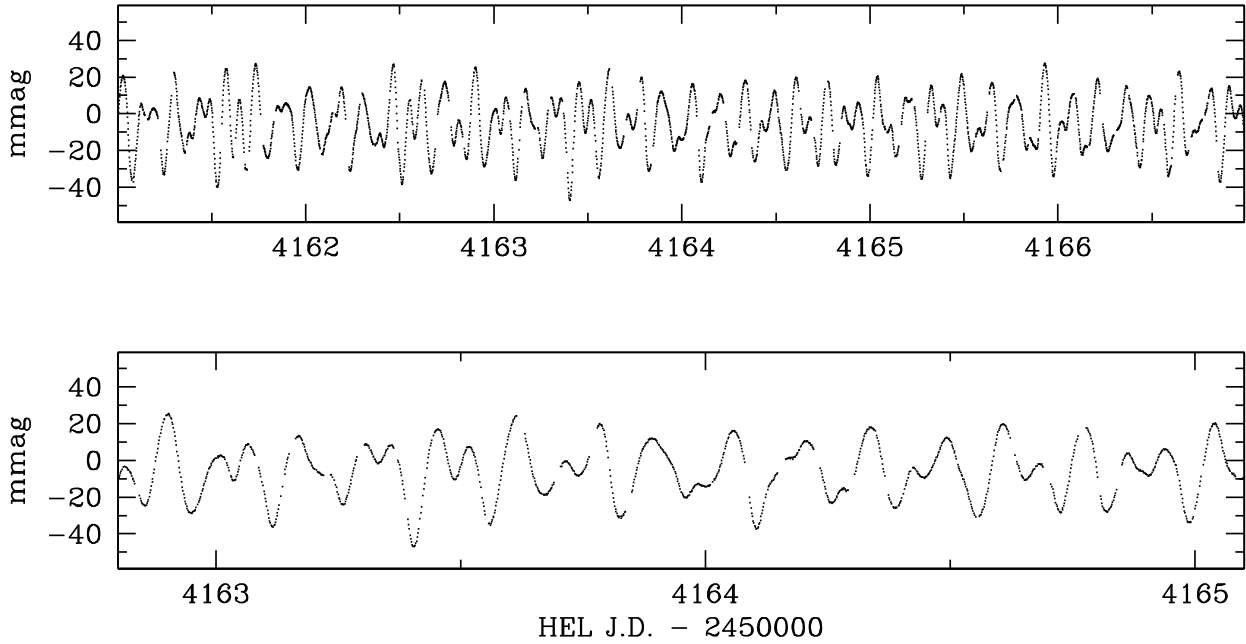


**Fig. 2.** Examples of the light curve of HD 50844 observed by CoRoT. *The lower panel is a zoom-in of a region of the upper panel.*

**Table 1.** Summary of the frequency detection.

| Detected frequencies | Amplitude | Residual rms [mmag] | SNR    | sig    |
|----------------------|-----------|---------------------|--------|--------|
| 0                    | –         | 13.63               | –      | –      |
| 1                    | 15.45     | 8.14                | 2060.5 | 4526.4 |
| 20                   | 0.64      | 2.85                | 85.5   | 175.6  |
| 60                   | 0.28      | 2.03                | 37.4   | 66.3   |
| 100                  | 0.20      | 1.74                | 26.7   | 46.9   |
| 200                  | 0.12      | 1.34                | 16.0   | 29.7   |
| 300                  | 0.09      | 1.11                | 12.0   | 23.4   |
| 500                  | 0.06      | 0.83                | 8.0    | 18.3   |
| 750                  | 0.04      | 0.61                | 5.3    | 15.7   |
| 1000                 | 0.03      | 0.48                | 4.0    | 12.6   |

20–30  $\text{d}^{-1}$  region is populated by the frequencies detected after the first 300.

It is worthwhile investigating how the detection of so many frequencies modifies the light curves. Figure 5 shows the light curve of HD 50844 at different stages of prewhitening. The multiperiodic nature of the original data (first panel) is obvious. For instance, the sine wave of the predominant frequency is almost cancelled by interference with other terms between HJD 2454159.5 and 2454159.6. Variability is still evident after removing 100 frequencies. This is an important step forward compared to previous ground-based and space observations. Also long-term oscillations are noticed at this level. After removing 250 frequencies, the residual light curve shows oscillations whose periods are around 0.05 d ( $\sim 20 \text{ d}^{-1}$ ; third panel). After removing even more frequencies, the oscillations progressively become more rapid and periods about 0.03 d ( $\sim 33 \text{ d}^{-1}$ ) are visible in the fourth and fifth panels of Fig. 5. This is another reflection of the distribution tail observed in the third panel of Fig. 4. It is quite evident that oscillations are still present after subtraction of 1000 terms. As shown in the last two columns of Table 1, after 1000 frequencies the SNR is around 4.0 and the Spectral Significance parameter (“sig”) of the SigSpec method is

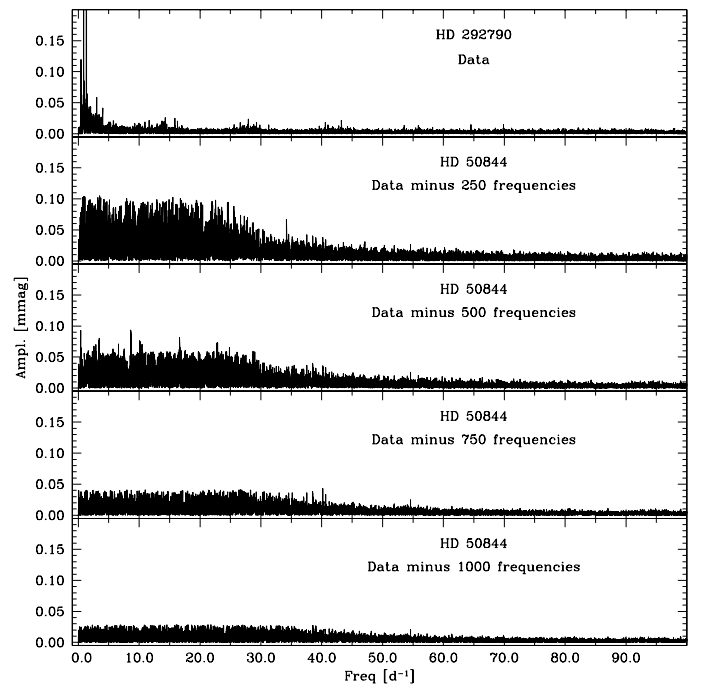


**Fig. 3.** For comparison purposes, the top panel shows the amplitude spectrum of the rotational variable HD 292790. This star has been observed by CoRoT simultaneously to HD 50844. The amplitude spectra of HD 50844 shown in the other panels indicate the extreme richness of the pulsational spectrum of this  $\delta$  Sct star: up to 1000 peaks are needed to make the residual spectrum of HD 50844 comparable to the original one of HD 292790.

around 12.6. The former is considered the acceptance limit in the frequency search algorithms such as Period04, while the latter is still above the threshold of the SigSpec method, i.e., 5.46. In a conservative way, we decided to stop the frequency search at this point, as it becomes more and more difficult to resolve new terms within our frequency resolution.

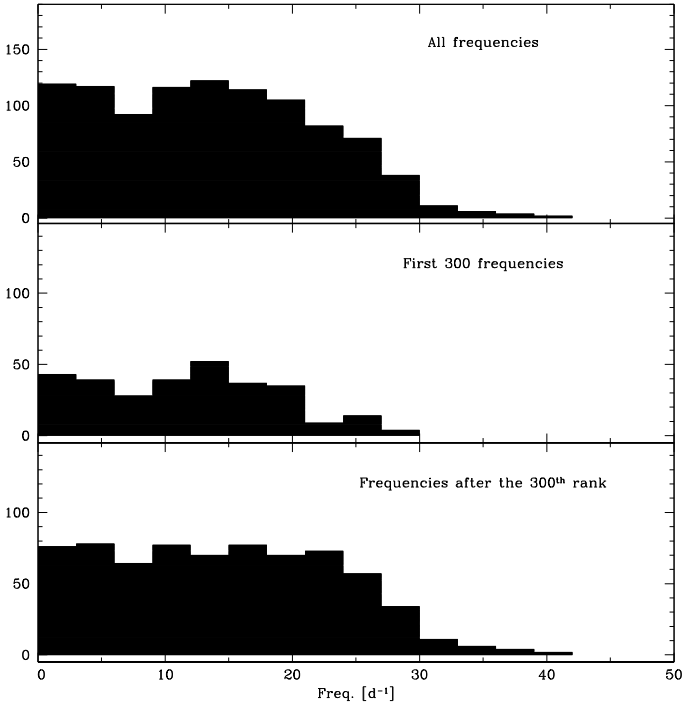


**Fig. 4.** Distribution of the frequencies. *Top panel:* histogram of all the 1000 frequencies. *Middle panel:* histogram of the first 300 frequencies in order of detection. *Bottom panel:* histogram of the frequencies detected after the first 300.

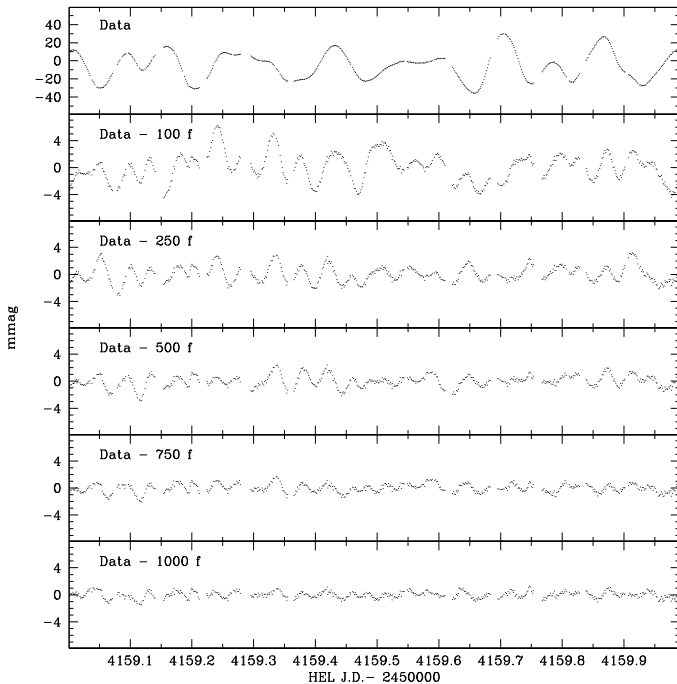


**Fig. 5.** The behaviour of the light curve of HD 50844 in the original data (*top panel*) and after subtracting the detected terms at different steps, where the time axis spans 1 d.

We considered it important to check the reliability of the frequency values determined until here. To do so, we compared the results from SigSpec and from the iterative-sine-wave fitting, considering an error range of  $0.005 \text{ d}^{-1}$  in frequency (i.e., a width 3.4 times narrower than  $1/\Delta T$ ). The cross-checks show an almost complete agreement on the values of the first

**Table 3.** First 20 frequencies identified in the amplitude spectrum.

| Term     | Frequency<br>[ $\text{d}^{-1}$ ] | Ampl.<br>[mmag] | Possible combination<br>terms                                  |
|----------|----------------------------------|-----------------|--|
| $f_1$    | 6.92528                          | 15.4539         | $f_{29} = 2f_1, f_{215} = 3f_1$                                |
| $f_2$    | 11.21669                         | 6.7220          | $f_{112} = f_1 + f_2, f_{123} = f_2 - f_1$<br>$f_{414} = 2f_2$ |
| $f_3$    | 11.25807                         | 4.0143          | $f_{159} = f_1 + f_3, f_{806} = f_3 - f_1$                     |
| $f_4$    | 12.84846                         | 3.3603          | $f_{129} = f_1 + f_4, f_{791} = f_4 - f_1$                     |
| $f_5$    | 12.23831                         | 3.3271          | $f_{217} = f_1 + f_5, f_{895} = f_5 - f_1$                     |
| $f_6$    | 14.44689                         | 3.1767          | $f_{118} = f_1 + f_6$  |
| $f_7$    | 13.27347                         | 2.6672          | $f_{356} = f_1 + f_7$  |
| $f_8$    | 13.35865                         | 2.3077          | $f_{149} = f_1 + f_8, f_{736} = f_8 - f_1$                     |
| $f_9$    | 11.75102                         | 1.4372          |  |
| $f_{10}$ | 5.26653                          | 1.1277          | $f_{64} = f_1 + f_{10}$  |
| $f_{11}$ | 14.46126                         | 1.0604          |  |
| $f_{12}$ | 14.43209                         | 0.9731          |  |
| $f_{13}$ | 9.95254                          | 0.9385          | $f_{781} = f_{13} - f_1$                                       |
| $f_{14}$ | 11.98380                         | 0.8268          | $f_{619} = f_1 + f_{14}$                                       |
| $f_{15}$ | 6.55624                          | 0.8259          | $f_{141} = f_1 + f_{15}$                                       |
| $f_{16}$ | 7.40446                          | 0.8099          |  |
| $f_{17}$ | 13.56880                         | 0.7768          | $f_{497} = f_{17} - f_1$                                       |
| $f_{18}$ | 10.26062                         | 0.7332          | $f_{309} = f_1 + f_{18}$                                       |
| $f_{19}$ | 5.78177                          | 0.7046          |  |
| $f_{20}$ | 6.62914                          | 0.6435          | $f_{494} = f_1 + f_{20}$                                       |

500 frequencies: 498 frequencies were found by both methods, whose 438 (88%) have an amplitude within the 20% range of tolerance. In particular, both methods correctly identified the first 462 frequencies within an interval of few units of  $10^{-4} \text{ d}^{-1}$ . These frequencies are listed in Table 2, which is available in electronic form at the CDS. The solutions of the two methods slowly diverge in the 500–1000th range because the differences will accumulate in the iterative process of the frequency extraction. Notwithstanding, the agreement is still satisfactory when considering all the 1000 frequencies: 953 were found by both methods, whose 805 with an amplitude within the 20% range.

We also performed another independent check. We created two subsets by considering the first and the second halves of the CoRoT timeseries. Again, we found a strong match between the frequencies obtained from the two subsets. However, we had to take the degradation of the frequency resolution into account and had to relax the error range. Therefore, the same analysis was repeated considering two subsets spanning the same time baseline, i.e., 50 days. The first subset was composed of the data in the time intervals 0.0–10.0 d and 30–50 d (0.0 d is the time of the first measurement) and the second subset consisted of the data in the intervals 10–30 d and 50–58 d. The two subsets have 823, 756, and 501 frequencies (out of 1000) in common considering a maximum separation of  $0.025 \text{ d}^{-1}$ ,  $0.020 \text{ d}^{-1}$  and  $0.010 \text{ d}^{-1}$ , respectively. Such large fractions of coincident terms suggest that they are more likely intrinsic to the star rather than due to transient instrumental effects. It is possible that some of the lower peaks originate from changes in amplitude or phase, or from other effects intrinsic to the star. In any case, the main conclusion of our analysis and related checks is that hundreds of terms – at least up to 1000 – are needed to explain the light variability of HD 50844. The detection of so many independent terms in the light variability of a  $\delta$  Sct star is a totally new result.

We also investigated the constancy of the highest amplitude terms, i.e., those listed in Table 3. We subdivided the CoRoT timeseries into five subsets, each spanning 11.6 d, and we calculated a least-squares fit of each subset. The amplitude of the predominant term  $f_1$  term is the most interesting to be investigated, since a low percentage of variability will immediately result in

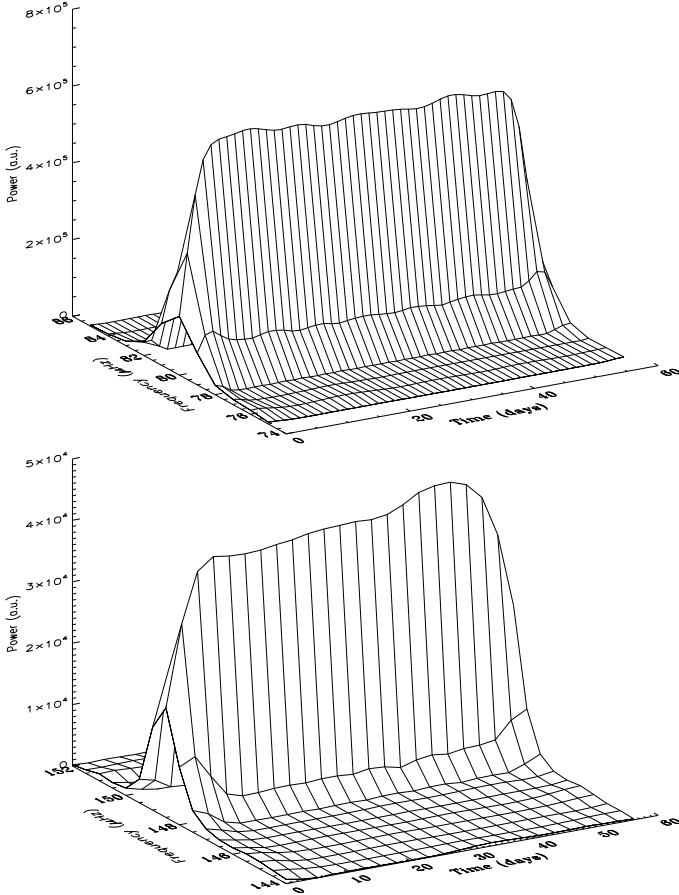


**Fig. 6.** Time-frequency analysis of the modes  $f_1 = 6.92 \text{ d}^{-1} = 80.1 \mu\text{Hz}$  (top) and  $f_4 = 12.85 \text{ d}^{-1} = 148.7 \mu\text{Hz}$  (bottom) with a frequency resolution of 2 and 1  $\mu\text{Hz}$ , respectively.

a detectable effect. The amplitude values span a full range of 0.10 mmag, with a formal error on each value of  $\pm 0.05$  mmag. Therefore, the amplitude of the  $f_1$  term can be considered constant. No significant amplitude variability has been detected in the other terms, except for  $f_6$ ,  $f_{11}$ , and  $f_{12}$ . These terms show evident amplitude and phase variations. This fact is a known effect induced by the interference of terms closer than the frequency resolution (Breger & Pamyatnykh 2006). A second investigation of the temporal behaviour of the amplitudes was performed using a time-frequency analysis (described in Baudin et al. 1994). This analysis is based on a Morlet wavelet with an adjustable frequency (and thus, time) resolution. If this resolution is greater than the frequency difference between two neighbouring terms, the power variation shows the beating described above. If the resolution is smaller than the frequency difference, the amplitude of the terms can be evaluated. We did not find any trace of variability of the amplitudes by performing this test on the terms considered above. The constant behaviour of the amplitudes is illustrated for the terms  $f_1$  and  $f_4$  in Fig. 6: the small variations observed are compatible with the influence of the noise.

Linear combinations of the terms having the highest amplitudes are commonly found in multiperiodic radial pulsators (Cepheids, RR Lyr, high amplitude  $\delta$  Sct stars), and are also observed in low amplitude  $\delta$  Sct stars, e.g., FG Vir (Breger et al. 2005). In the solution of HD 50844 we find some frequencies with a high rank of detection that could be explained as a linear combination of a frequency with a low rank and the first, predominant term  $f_1$  (Table 3). However, we cannot rule out that

these high-rank frequencies are actually independent modes, excited by resonance mechanisms or even intrinsically excited.

## 4. Ground-based observations

### 4.1. High-resolution spectroscopy: line profile variations

The spectroscopic observations were completed from January 2 to 28, 2007 with the FEROS instrument mounted at the 2.2-m ESO/MPI telescope, La Silla, Chile. The spectral resolution of FEROS is  $R \sim 48\,000$ . We obtained 232 spectra in 14 nights. The exposure time was set to 900 s and the signal-to-noise ratios (SNRs) ranged from 150 to 210. The spectra were reduced using an improved version of the standard FEROS pipeline, written in MIDAS and developed by Rainer (2003). In addition to the individual line profiles, we considered the mean profiles computed using the least-squares deconvolution (LSD) method (Donati et al. 1997). When calculating the LSD profiles, the spectral region between 4150 and 5800  $\text{\AA}$  was used, taking care to omit the intervals containing the  $H_\beta$  and  $H_\gamma$  lines. By calculating a single line profile with an average SNR of about 1200 for each spectrum, we increased the original SNR of the individual spectra by a factor of six. The mean barycentric radial velocity of the star is  $-10.8 \pm 0.2 \text{ km s}^{-1}$ . We also derived a  $v \sin i$  value of  $58 \pm 2 \text{ km s}^{-1}$  from *i*) the first zero-point position of the Fourier transform for the mean LSD profile and *ii*) a nonlinear least-squares fit of an intrinsic profile computed for the stellar physical parameters of HD 50844 convolved with a rotationally broadened one.

Before presenting the results of the frequency analysis, we clearly note that the shorter baseline of the spectroscopic observations (27 d) implies a frequency resolution worse than that of the CoRoT photometric data. The power spectrum of the line profile variations (LPVs) detected in the spectroscopic data is shown in the bottom panel of Fig. 1. Since the observations are single-site, the spectral window is more complicated because of the presence of relevant aliases at integer values of  $\text{d}^{-1}$  from the real peak. These facts result in uncertainties on the amplitudes and on the reliable detection of the spectroscopic frequencies. Nevertheless, the study of the LPVs is of paramount importance for corroborating and complementing the photometric results, as suggested by the different appearances of the photometric and spectroscopic power spectra (Fig. 1, middle and bottom panels).

The spectroscopic frequencies were searched for by analysing the LPVs by means of the pixel-by-pixel technique (Mantegazza 2000; Zima 2006). Table 4 lists the terms detected in order of decreasing spectroscopic amplitude (in continuum units as defined by Zima 2006), which is a measurement of the contribution of the given term to the line profile variability. We detected 27 terms with an SNR higher than 4.0 and 3 terms with  $3.1 < \text{SNR} < 3.5$  (see Table 4). The three modes with  $3.1 < \text{SNR} < 3.5$  were also considered in the LPV analysis since they are associated with well-defined CoRoT frequencies. The spectroscopic frequencies were associated with the closest frequency detected in all the photometric solutions. In the few cases in doubt (4 out of 30), the term with the largest amplitude was preferred. This assumption did not modify the subsequent ( $l, m$ ) identification since the amplitude and the phase diagrams did not appreciably change with the frequency used to fold the spectroscopic data. A different association with a photometric term would have modified the photometric amplitude, but this parameter cannot be used in the spectroscopic mode identification.

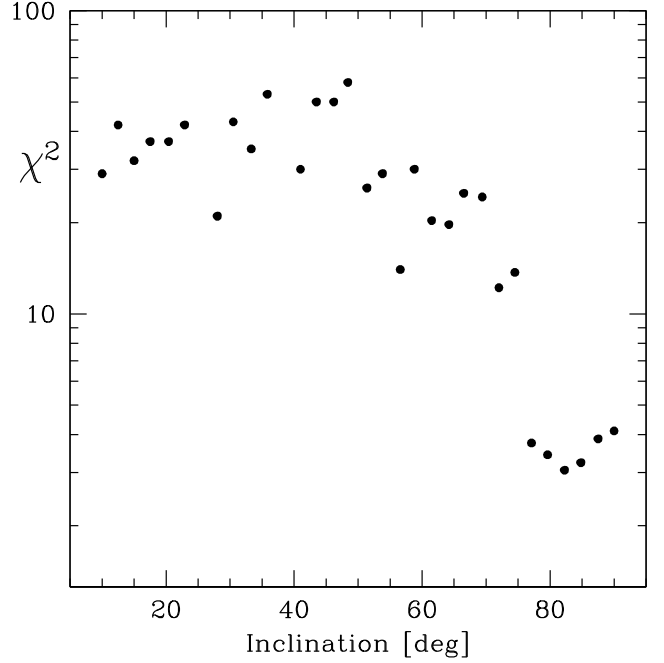
The mode identification was performed by fitting the amplitude and phase variations of each mode across the line profile (Mantegazza 2000) by using the software FAMIAS

**Table 4.** The frequencies identified in high-resolution spectroscopy.

| Term      | Frequency<br>[d <sup>-1</sup> ] | Spectr.<br>Ampl. | SNR  | $\ell, m$ | EW<br>[km s <sup>-1</sup> ] | RV<br>[km s <sup>-1</sup> ] |
|-----------|---------------------------------|------------------|------|-----------|-----------------------------|-----------------------------|
| $f_{12}$  | 14.43209                        | 0.27             | 28.6 | 4, 2      |                             | 0.10                        |
| $f_{22}$  | 14.47568                        | 0.24             | 22.2 | 3, 1      |                             |                             |
| $f_6$     | 14.44689                        | 0.24             | 23.0 | 4, 3      | 0.009                       |                             |
| $f_7$     | 13.27347                        | 0.18             | 15.8 | 3, 2      | 0.009                       |                             |
| $f_3$     | 11.25807                        | 0.15             | 13.1 | 5, 1      |                             |                             |
| $f_4$     | 12.84846                        | 0.14             | 19.5 | 3, 3      | 0.008                       | 0.52                        |
| $f_{243}$ | 15.54114                        | 0.14             | 14.6 | 9, 2      |                             |                             |
| $f_{50}$  | 15.22329                        | 0.13             | 10.9 | 12, 10    |                             |                             |
| $f_{18}$  | 10.26062                        | 0.13             | 12.5 | 5, 0      |                             |                             |
| $f_{29}$  | 13.85029                        | 0.13             | 13.4 | $2f_1$    |                             |                             |
| $f_{69}$  | 13.16891                        | 0.12             | 13.0 | 8, 2      |                             |                             |
| $f_{452}$ | 16.50451                        | 0.12             | 9.2  | 14, 14    |                             |                             |
| $f_8$     | 13.35865                        | 0.10             | 8.9  | 5, 3      |                             | 0.11                        |
| $f_1$     | 6.92528                         | 0.11             | 5.0  | 0, 0      | 0.061                       | 0.72                        |
| $f_2$     | 11.21669                        | 0.11             | 9.5  | 3, 1      | 0.022                       | 0.39                        |
| $f_{51}$  | 11.64327                        | 0.10             | 9.3  | 8, 5      |                             | 0.08                        |
| $f_{521}$ | 15.12491                        | 0.10             | 8.1  | 7, 4      |                             |                             |
| $f_{10}$  | 5.26653                         | 0.09             | 4.2  | 2, -2     |                             | 0.08                        |
| $f_{77}$  | 15.80497                        | 0.08             | 6.2  | 4, 3      |                             |                             |
| $f_9$     | 11.75102                        | 0.08             | 6.4  | 11, 7     |                             | 0.05                        |
| $f_{81}$  | 19.71529                        | 0.07             | 4.2  | 12, 8     |                             |                             |
| $f_{84}$  | 9.61191                         | 0.06             | 4.1  | 10, 4     |                             |                             |
| $f_{27}$  | 5.67472                         | 0.06             | 3.1  | 4, -2     |                             |                             |
| $f_{71}$  | 14.99570                        | 0.06             | 6.7  | 6, 3      |                             |                             |
| $f_{46}$  | 19.75025                        | 0.06             | 4.1  | 14, 12    |                             |                             |
| $f_{43}$  | 5.04299                         | 0.05             | 3.5  | 4, -2     |                             | 0.12                        |
| $f_{32}$  | 5.49058                         | 0.05             | 3.4  | 5, -2     |                             |                             |
| $f_{44}$  | 14.60061                        | 0.05             | 4.1  | 6, 4      |                             |                             |
| $f_5$     | 12.23831                        | –                | –    | –         | 0.018                       | 0.45                        |
| $f_{11}$  | 14.46126                        | –                | –    | –         |                             | 0.20                        |
| $f_{13}$  | 9.95254                         | –                | –    | –         |                             | 0.10                        |
| $f_{30}$  | 5.41862                         | –                | –    | –         |                             | 0.08                        |
| $f_{19}$  | 5.78177                         | –                | –    | –         |                             | 0.08                        |
| Error     |                                 | 0.02             |      |           | 0.002                       | 0.02                        |

(Zima 2008). The identified  $(\ell, m)$  values are listed in Table 4. In the  $(\ell, m)$  couples, the negative  $m$  values indicate retrograde modes. Uncertainties are estimated to be  $\pm 1$  for the degree  $\ell$  and  $\pm 2$  for the order  $m$ . They are larger in the cases of the modes  $f_{12}$  and, in particular,  $f_{22}$  and  $f_6$ , since they are very close in frequency. Also the nonsignificant detection of  $f_{11}$  is probably a problem related to the low resolution in the spectroscopic data. Mainly tesseral modes were detected, but also a couple of sectoral modes were found. This technique also returned a reliable estimate of the inclination angle, i.e.,  $i = 82 \pm 4$  deg (Fig. 7). Therefore, HD 50844 is seen almost equator-on. The associated equatorial rotational velocity is not significantly different from the  $v \sin i$  value derived above. This particular orientation explains why only one axisymmetric mode (i.e.,  $f_{18}$ , Table 4) was observed: these modes produce marginal variations along our line of sight.

An independent search for frequencies was performed on the timeseries defined by the 0th (equivalent width, EW) and 1st (radial velocity,  $\langle v \rangle$ ) order moments. Since these quantities are integrated over the whole stellar disk, they are more sensitive to reveal low-degree modes. The amplitudes of the frequencies, detected in both moments by the Period04 (Lenz & Breger 2005) method, are listed in Table 4. We recover in the EW and  $\langle v \rangle$  variations (bottom of Table 4) some of the terms with a large photometric amplitude that have been missed in the LPV analysis, because of their intrinsic low spectroscopic amplitude. Since they were detected in the first moments, we can speculate that it probably concerns low-degree modes.

**Fig. 7.** Behaviour of the  $\chi^2$  values, obtained by fitting all the 30 spectroscopic modes to the LSD profiles, each time keeping the same fixed value for the inclination angle.

The six frequencies detected in the EW variations correspond to six out of the seven first photometric frequencies. The term  $f_3$  is probably missing because it is not well-resolved from  $f_2$  and  $f_5 - 1$  d<sup>-1</sup>. The correlation between the terms found in the 1<sup>st</sup> moment and those detected in the CoRoT photometric data is not as clear as in the case of the 0<sup>th</sup> moment. We note that the frequency  $13.85029$  d<sup>-1</sup> =  $2f_1$  was detected in the pixel-to-pixel variations (Table 4). Does it really concern the first harmonic of  $f_1$  or is it an independent mode excited by resonance? We tested the hypothesis following the method described by Telting & Schrijvers (1997), which states that a frequency is a first harmonic if the phase difference  $\psi_{01} = 2\psi_0 - \psi_1$  between the line-centre phases of the two frequencies is  $1.50 \pi$  rad. Because we measure  $\psi_{01} = 1.58 \pi \pm 0.19$  rad, we conclude that  $13.85029$  d<sup>-1</sup> is indeed the first harmonic of  $f_1$ .

The main goal of the spectroscopic observations is to answer the crucial question about the huge number of frequencies detected in the CoRoT photometric data: is the large number of photometric terms related to the visibility not only of low-degree modes but also of high-degree modes? To investigate this we focus on the mode identification results, as derived from the high-resolution data, presented in Table 4. In Fig. 8 we plot the identified degree  $\ell$  in function of order  $m$ . This figure shows that the high-degree modes also tend to have a high order  $m$ . The highest detected degree is  $\ell = 14$ . This observational fact tells us that we have at least 235 possible modes of pulsation for a given radial order  $n$ . A few different radial orders are sufficient for explaining the 1000 frequencies detected in the CoRoT photometric timeseries of HD 50844. On the other hand, we know from CoRoT photometry that the frequency values higher than  $30$  d<sup>-1</sup> are observed after the 300<sup>th</sup> rank of detection, i.e., with very low amplitudes. The observed spectroscopic frequencies have  $f < 20$  d<sup>-1</sup>. We still miss the spectroscopic counterpart of the  $20 < f < 50$  d<sup>-1</sup> region. Such a region could be filled by modes with high radial orders  $n$ , which are shifted toward higher frequencies than those of the low orders.

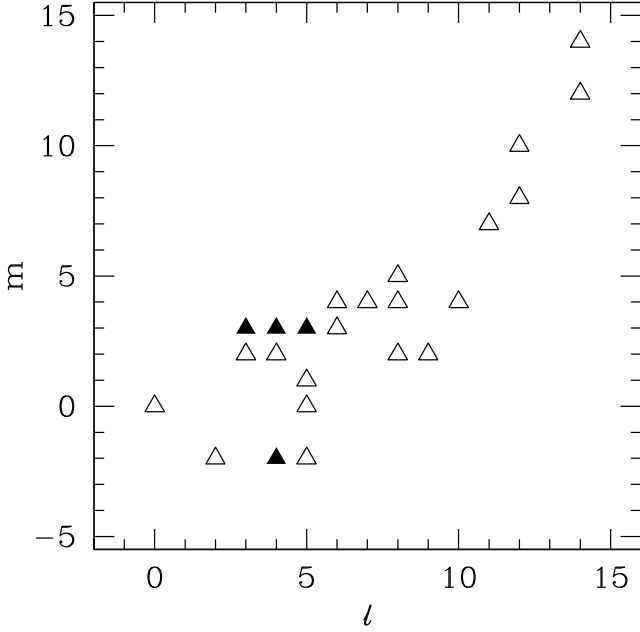


**Fig. 8.** Identification of the  $(\ell, m)$  couples from high-resolution spectroscopy. Open triangles: one term with that  $(\ell, m)$  identification. Filled triangles: two terms with that  $(\ell, m)$  identification.

**Table 5.** Mean LTE abundances  $\log \epsilon(\text{El})$  along with the uncertainties,  $\sigma$ , with solar abundances determined by Grevesse et al. (2007).

| Element | Z  | $\log \epsilon(\text{El})$ | $\sigma$ | Sun  |
|---------|----|----------------------------|----------|------|
| C       | 6  | 8.45                       | 0.130    | 8.39 |
| N       | 8  | 8.72                       | 0.102    | 8.66 |
| Na      | 11 | 5.75                       | 0.097    | 6.17 |
| Mg      | 12 | 7.02                       | 0.113    | 7.53 |
| Si      | 14 | 6.95                       | 0.386    | 7.51 |
| S       | 16 | 7.25                       | 0.054    | 7.14 |
| Ca      | 20 | 5.91                       | 0.112    | 6.31 |
| Sc      | 21 | 2.56                       | 0.103    | 3.17 |
| Ti      | 22 | 4.40                       | 0.159    | 4.90 |
| V       | 23 | 3.38                       | 0.146    | 4.00 |
| Cr      | 24 | 5.10                       | 0.140    | 5.64 |
| Mn      | 25 | 4.68                       | 0.157    | 5.39 |
| Fe      | 26 | 6.71                       | 0.126    | 7.45 |
| Co      | 27 | 4.89                       | 0.098    | 4.92 |
| Ni      | 28 | 5.53                       | 0.151    | 6.23 |
| Cu      | 29 | 3.52                       | 0.018    | 4.21 |
| Zn      | 30 | 3.93                       | 0.079    | 4.60 |
| Y       | 39 | 1.67                       | 0.099    | 2.21 |
| Zr      | 40 | 2.37                       | 0.458    | 2.58 |
| Ba      | 56 | 1.91                       | 0.170    | 2.17 |
| La      | 57 | 0.483                      | 0.126    | 1.13 |
| Ce      | 58 | 0.292                      | 0.436    | 1.70 |

The excitation of the almost totality of the modes allowed within a narrow radial order interval and its possible extension to a wide range of radial orders can explain the presence of 1000 terms in quite a natural way. In either case, we can state that the huge number of photometric terms are plausible since the spectroscopic data are confirming that we are observing modes with high  $(\ell, m)$  values. In turn, this means that the cancellation effects for modes up to  $\ell \sim 14$  are not working and that these modes are able to produce a net flux measurable at the  $10^{-5}$  mag level.

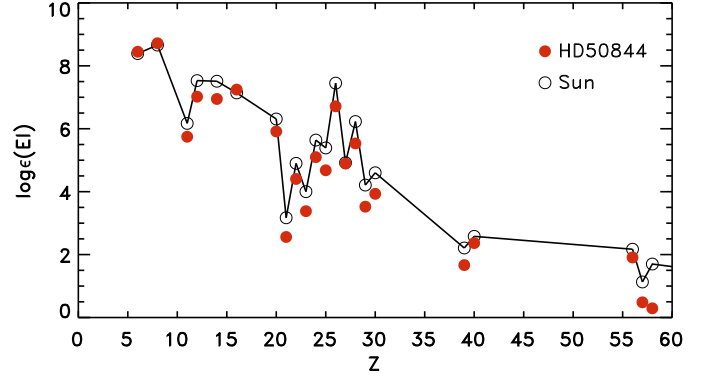


**Fig. 9.** Element abundances of HD 50844 derived from FEROS spectra compared to the solar values (Grevesse et al. 2007).

#### 4.2. High-resolution spectroscopy: abundance analysis

In addition to the LPV analysis, the FEROS spectra were used to determine the abundances of the elements. The atmospheric models were computed with the line-blanketed LTE ATLAS9 code (Kurucz 1993), which handles line opacity with the opacity distribution function. The synthetic spectra were computed with the SYNTHE code (Kurucz 1993). The stellar-line identification and the abundance analysis were performed on the basis of the VALD lines list (Kupka et al. 2000). The mean LTE abundances  $\log \epsilon(\text{El})$  (by convention,  $\log \epsilon[\text{H}] = 12$ ), along with the uncertainties determined as  $\sigma = \sqrt{\sigma_T^2 + \sigma_{\log g}^2}$  are reported in Table 5. The atmospheric parameters  $T_{\text{eff}} = 7400$  K,  $\log g = 3.6$  and  $\xi = 2$  km  $\text{s}^{-1}$  were adopted. To determine the uncertainties connected with effective temperature and surface gravity, we calculated the abundances for atmospheric models with  $T_{\text{eff}} = \pm 200$  K and  $\log g = \pm 0.2$ .

As a general result, HD 50844 is a slightly metal-deficient star. However, Table 5 shows how the abundances of elements as C, N, and S in the HD 50844 atmosphere are very similar to those of the Sun, while other elements are underabundant (see also Fig. 9). Such an abundance pattern is typical of  $\lambda$  Boo stars (Pauzen 2004). With respect to the claimed spectroscopic binarity of these stars (Gerbaldi et al. 2003), we did not find any evidence of a second component in the FEROS spectra, and we did not detect a long-term radial velocity drift that could be ascribed to an orbital motion.

#### 4.3. Multicolour photometry

The importance of colour information to estimate the degree  $\ell$  of the modes is well-known (Garrido 2000); therefore, we observed HD 50844 in Stromgren *uvby* photometry to accompany the CoRoT white-light photometry. Several campaigns were carried out at S. Pedro Mártir and Sierra Nevada observatories, using twin Danish photometers. The multicolour observations span 743 d. The campaigns started when the IR01 pointing was decided and continued after the CoRoT observations. The final *uvby* dataset consists of 1496 datapoints, collected in 66 nights for a total survey of 317.4 h. Unfortunately, the space and ground-based observing windows are not simultaneous. The spectral window of the ground-based data is characterized by several alias peaks (at integer values of  $\text{d}^{-1}$  and  $\text{ys}^{-1}$  of the central peak) and the true peaks could only be identified knowing the CoRoT solution. We considered the first 20 CoRoT frequencies and refined their values by performing a least-squares fit of

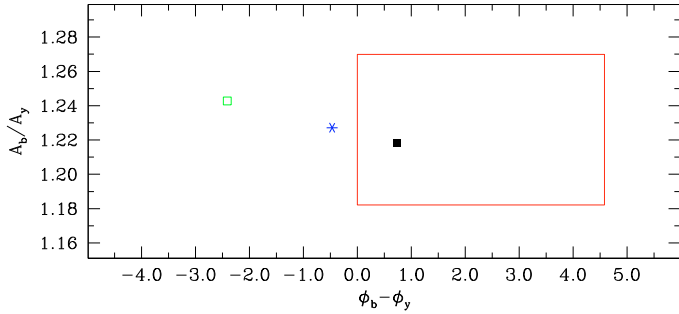


**Fig. 10.** Comparison between theoretical predictions and multicolour photometric observations for  $f_1$ , the mode with the largest photometric amplitude. Amplitude ratios vs. phase differences (in degrees) in  $b$  and  $y$  colours are shown. Red large square is the observed errorbox. Points represent theoretical predictions for spherical degree  $\ell = 0$  (black filled square),  $\ell = 1$  (blue star), and  $\ell = 2$  (green open square).

the data in the  $v$  colour, i.e., the one with the largest amplitude. This step was necessary since the time baseline of the *wby* data is much longer than that of the CoRoT data. The first 13 frequencies resulted in a significant  $v$ -amplitude. The  $v$ -amplitude of the  $f_1$  term is  $22.2 \pm 0.3$  mmag, while those of the others are much lower (e.g., 8.0 mmag for  $f_2$  and 1.70 mmag for  $f_{13}$ ).

We calculated the amplitude ratios and the phase shifts by using the  $y$  colour as the reference system (Garrido 2000). They were compared with the theoretical predictions computed using the non-adiabatic pulsational code GraCo (Moya & Garrido 2008). The immediate result is that the predominant term  $f_1 = 6.92$  d $^{-1}$  is characterized by positive phase shifts (i.e.,  $\phi_{u,v,b} - \phi_y > 0.0$ ). This puts a very tight constraint on the mode identification, since only the radial ( $\ell = 0$ ) mode shows positive phase shifts in the  $\phi_b - \phi_y$  case (Fig. 10). On the other hand, the comparison between the observed and the calculated values does not supply conclusive mode identifications in the cases of the other terms.

To further investigate the  $f_1$  mode identification, we note that the harmonics  $2f_1 = f_{29}$  (amplitude 0.56 mmag) and  $3f_1 = f_{215}$  (0.12 mmag) have been detected in the CoRoT data. The observed values differ from the exact multiples of  $f_1$  by  $3 \times 10^{-4}$  and  $1 \times 10^{-3}$  d $^{-1}$ , respectively. Both the  $\phi_{21} = 4.04$  rad and the  $\phi_{31} = 2.11$  rad Fourier parameters are very similar to those observed in high amplitude  $\delta$  Sct stars (Figs. 4 and 5 in Poretti 2001), known to pulsate in the fundamental (rarely in the first overtone) radial mode. Identification of  $f_1$  as a radial mode is also consistent with being the highest amplitude term both in radial velocity and in equivalent width. Although a nonradial mode could display such large variations, such variations are usually connected with the large displacements typical of radial modes. The mode identification of the  $f_1$  term from the spectroscopic data was not trivial since we had to take the harmonic  $2f_1$  and the EW variations into account. The FAMIAS method returns two possible  $(\ell, m)$  couples, i.e.,  $(0, 0)$  and  $(2, 0)$ . When considering both the spectroscopic and the photometric identifications, we can consider the  $f_1$  term as the fundamental radial mode.

## 5. The seismic inferences

The discussion of the number of excited frequencies in  $\delta$  Sct stars has followed a particular pattern. At the beginning of the observational efforts to discover as many modes as possible (Poretti 2000; Breger 2000), the number of detected frequencies was less than expected and a kind of selection effect in exciting

modes/damping amplitudes was claimed (Guzik et al. 2000, and, more recently, Breger et al. 2009). Garrido & Poretti (2004) suggest that the problem was mainly of an SNR nature. They stressed how the number of detected terms in the science case of FG Vir follows an exponential behaviour as a function of the observational technique used, namely from single-site observations in a few nights to multisite observations in several years. In a certain sense, they correctly predicted that a long-term, high-precision space mission as CoRoT would allow access to the distribution of the amplitudes down to  $10^{-5}$ – $10^{-6}$  mag, allowing the harvest of a multitude of modes. That the distribution of the frequencies is quite uniform in the 0–20 d $^{-1}$  region (Fig. 4) implies that modes are excited at lower frequencies than that of the fundamental radial mode, i.e.,  $f < 6.9$  d $^{-1}$ . The peaks with  $f < 3$  d $^{-1}$  can be enhanced by an incomplete removal of the instrumental drift. The spectrum of HD 292790 (Fig. 3, top panel) shows a noise level below 0.05 mmag in this region and therefore this contamination should become important only after the 600th frequency (see Table 1). We can argue from the CoRoT timeseries on HD 50844 that gravity and mixed modes are quite common in  $\delta$  Sct stars.

The frequency set obtained from the CoRoT timeseries of HD 50844 allows us to investigate the problem of the regular spacings in the frequency spectrum of  $\delta$  Sct stars. There have been several claims that such spacings will be modified by nonlinear effects and mixed modes, especially in evolved stars (Christensen-Dalsgaard 2000; Goupil & Dziembowski 2000; Guzik et al. 2000). This hint is confirmed by the frequency spectrum of HD 50844, which does not supply any reliable indication of the regular spacings detected in solar-like pulsators (e.g., Michel et al. 2008).

As a first attempt to model the scientific case of HD 50844, equilibrium models representative of the star have been calculated with the evolutionary code CESAM (Morel 1997), taking first-order effects of rotation into account. Such models (the so-called pseudo-rotating models) include the spherically averaged contribution of the centrifugal acceleration by means of an effective gravity. The nonspherical components of the centrifugal acceleration (not considered in the equilibrium models) are included in the adiabatic oscillation computations by means of a linear perturbation analysis (Suárez et al. 2006). Figure 11 shows the models within the uncertainty box in  $T_{\text{eff}}$  and  $\log g$ . The models, evolved considering the local conservation of the angular momentum, are able to return a surface rotational velocity around 60 km s $^{-1}$  (i.e., the value obtained from  $v \sin i$  taking  $i = 80$  deg as suggested by the analyses of the line profile variations) starting from a value of 75 km s $^{-1}$  on the ZAMS. We can also compute the fundamental radial mode of our models using the code GraCo (Moya & Garrido 2008): the darker box in Fig. 11 marks the cases matching the observed value  $f_1$ . When considering the slightly metal deficient content of HD 50844, we can argue that the models suggest a mass between 1.65 and 1.80  $M_{\odot}$ .

## 6. Conclusions

The exploitation of the CoRoT photometric timeseries of HD 50844 resulted in a very complex and intriguing task, also giving a completely new picture of the pulsational content of  $\delta$  Sct stars. We demonstrated that the light curve of HD 50844 can be explained by the presence of hundreds of excited terms. Classical checks such as using different software packages, subdividing the timeseries into different subsets, carefully inspecting the residuals, and comparing with other similar targets

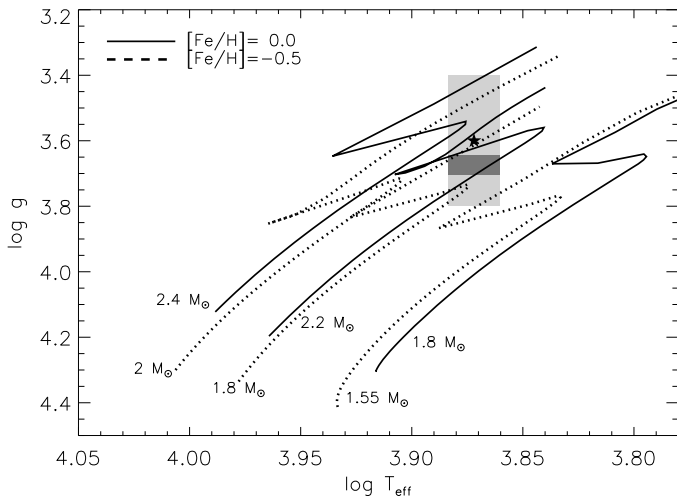


**Fig. 11.** HR diagram containing several evolutionary tracks of representative models of the star. The shaded area represents the observational uncertainties in effective temperature and gravity. The models in the darker area have a fundamental radial mode equal to  $f_1 = 6.925 \text{ d}^{-1}$ . The filled star represents the observational average location of HD 50844 in the diagram. Continuous lines represent tracks of evolved models with a solar metallic content, whereas dotted lines represent evolutionary tracks of submetallic models; the latter are more representative of the HD 50844 case.

observed by CoRoT, together confirm this issue. High-resolution spectra support the excitation of modes having a very high degree  $\ell$  (up to  $\ell = 14$ ), thus providing an observational explanation for the richness of the frequency spectrum. Such a large number of modes of different  $\ell$  simultaneously excited is among plausible features suggested by theoretical works (e.g., Balona & Dziembowski 1999). An immediate conclusion is that the cancellation effects are not sufficient in removing the variations of the flux integrated over the whole stellar disk; Daszyńska-Daszkiewicz et al. (2006) correctly predicted this extension to high degrees of the modes extracted from high-precision photometric timeseries. We should keep in mind that the CoRoT performances and the continuous monitoring allow detection of amplitudes of about  $10^{-5}$  mag without significant aliasing effects, which is a totally new perspective.

The case of HD 50844 seems to match the theoretical picture featuring a very large number of excited modes with amplitudes limited by a saturation mechanism of the  $\kappa$  mechanism. This confirms that the observation of  $\delta$  Sct stars with CoRoT will allow us to address the longstanding problem of amplitude distribution and the potential existence of mode selection processes in the  $\delta$  Sct instability strip. We note that HD 50844 probably does not constitute a “standard” scientific case of a  $\delta$  Sct star, because it is located on the TAMS, probably belongs to the class of  $\lambda$  Boo stars (i.e., showing atmospheric particularities), and it is seen almost equator-on. Nevertheless, seismic models that were able to reproduce the position of HD 50844 in the HR diagram and its measured rotational velocity were calculated.

HD 50844 has for the first time disclosed the intrinsic complexity of frequency spectra of intermediate-mass stars in the lower part of the instability strip. It is quite evident that, after these first CoRoT observations, we must look at  $\delta$  Sct stars in a completely new way. We have to realize that ground-based observations were only able to observe the tip of the iceberg, while the larger part of the modes have remained undetected.

**Acknowledgements.** The FEROS data are being obtained as part of the ESO Large Programme LP178.D-0361 (PI.: E. Poretti). The authors wish to thank the anonymous referee for useful comments. Mode identification results were obtained with the software package FAMIAS developed in the framework of the FP6 Coordination Action Helio- and Asteroseismology (HELAS; <http://www.helas-eu.org/>). W.Z. was supported by the FP6 European Coordination Action HELAS and by the Research Council of the University of Leuven under grant GOA/2008/04. This work was supported by the Italian ESS project, contract ASI/INAF I/015/07/0, WP 03170, and by the Hungarian ESA PECS project No. 98022. K.U. acknowledges financial support from a *European Community Marie Curie Intra-European Fellowship*, contract number MEIF-CT-2006-024476. P.J.A. acknowledges financial support from a *Ramon y Cajal* contract of the Spanish Ministry of Education and Science. A.M. acknowledges financial support from a *Juan de la Cierva* contract of the Spanish Ministry of Science and Technology. S.M.R. acknowledges a *Retorno de Doctores* contract financed by the Junta de Andalucía and Instituto de Astrofísica de Andalucía for carrying out observing campaigns for CoRoT targets at Sierra Nevada Observatory. E.N. acknowledges financial support of the N203 302635 grant from the MNISW.

## References

- Auvergne, M., Bodin, P., Boissard, L., et al. 2009, *A&A*, 506, 411  
 Balona, L. A., & Dziembowski, W. A. 1999, *MNRAS*, 309, 221  
 Baudin, F., Gabriel, A., & Gibert, D. 1994, *A&A*, 285, L29  
 Breger, M. 2000, in *Delta Scuti and Related Stars*, ed. M. Breger, & M. H. Montgomery, ASP Conf. Ser., 210, 3  
 Breger, M., & Pamyatnykh, A. A. 2006, *MNRAS*, 368, 571  
 Breger, M., Lenz, P., Antoci, V., et al. 2005, *A&A*, 435, 955  
 Breger, M., Lenz, P., & Pamyatnykh, A. A. 2009, *MNRAS*, 396, 291  
 Christensen-Dalsgaard, J. 2000, in *Delta Scuti and Related Stars*, ed. M. Breger, & M. H. Montgomery, ASP Conf. Ser., 210, 187  
 Daszyńska-Daszkiewicz, J., Dziembowski, W. A., & Pamyatnykh, A. A. 2006, *Mem. SAI*, 77, 113  
 Donati, J.-F., Semel, M., Carter, B. D., Rees, D. E., & Collier Cameron, A. 1997, *MNRAS*, 291, 658  
 Garrido, R. 2000, in *Delta Scuti and Related Stars*, ed. M. Breger, & M. H. Montgomery, ASP Conf. Ser., 210, 67  
 Garrido, R., & Poretti, E. 2004, in *Variable Stars in the Local Group*, ed. D. W. Kurtz, & K. R. Pollard, IAU Colloq., 193, ASP Conf. Ser., 310, 560  
 Gerbaldi, M., Faraggiana, R., & Lai, O. 2003, *A&A*, 412, 447  
 Goupil, M.-J., & Dziembowski, W. A. 2000, in *Delta Scuti and Related Stars*, ed. M. Breger, & M. H. Montgomery, ASP Conf. Ser., 210, 267  
 Grevesse, N., Asplund, M., & Sauval, A. J. 2007, *Space Sci. Rev.*, 130, 105  
 Guzik, J. A., Bradley, P. A., & Templeton, M. R. 2000, in *Delta Scuti and Related Stars*, ed. M. Breger, & M. H. Montgomery, ASP Conf. Ser., 210, 247  
 Kupka, F. G., Ryabchikova, T. A., Piskunov, N. E., et al. 2000, *Baltic Astron.*, 9, 590  
 Kurucz, R. L. 1993, *ATLAS9, Stellar Atmosphere Programs*, CD-ROM, 18, Smithsonian Astrophysical Observatory  
 Lefèvre, L., & Chené, A. N. 2009, *CoAst*, in press  
 Lenz, P., & Breger, M. 2005, *CoAst*, 146, 53  
 Mantegazza, L. 2000, in *Delta Scuti and Related Stars*, ed. M. Breger, & M. H. Montgomery, ASP Conf. Ser., 210, 138  
 Michel, E., Baglin, A., Auvergne, M., et al. 2008, *Science*, 322, 558  
 Morel, P. 1997, *A&AS*, 124, 597  
 Moya, A., & Garrido, R. 2008, *Ap&SS*, 316, 129  
 Paunzen, E. 2004, in *The A-Star Puzzle*, ed. J. Zverko, J. Ziznovsky, S. J. Adelman, & W. W. Weiss (Cambridge University Press), Proc. IAU Symp., 224, 443  
 Poretti, E. 2000, in *Delta Scuti and Related Stars*, ed. M. Breger, & M. H. Montgomery, ASP Conf. Ser., 210, 45  
 Poretti, E. 2001, *A&A*, 371, 986  
 Poretti, E., Alonso, R., Amado, P. J., et al. 2005, *AJ*, 129, 2461  
 Rainer, M. 2003, *Laurea Thesis* (in Italian), Università degli Studi di Milano  
 Reegen, P. 2007, *A&A*, 467, 1353  
 Suárez, J. C., Goupil, M. J., & Morel, P. 2006, *A&A*, 449, 673  
 Telting, J. H., & Schrijvers, C. 1997, *A&A*, 317, 723  
 Uytterhoeven, K., Mathias, P., Poretti, E., et al. 2008, *A&A*, 489, 1213  
 Vaníček, P. 1971, *Ap&SS*, 12, 10  
 Zima, W. 2006, *A&A*, 455, 227  
 Zima, W. 2008, *CoAst*, 155, 17